CHAPTER 4
SCREENING AND CHARACTERIZATION OF SELECTED IONIC LIQUIDS

4.0 Overview

In this chapter the screening of potential ILs for extractive desulfurization process using AI and DBE assisted COSMO-RS are pondered in detail. Then, the potential ILs were synthesized and characterized accordingly for structure confirmation, elemental analysis, water and halide content together with density and refractive index. Thermophysical properties were also calculated including molecular volume, lattice potential energy and absolute entropy.

4.1 Comparison Study of Interaction Mechanism between ILs and Sulfur Compounds

In the initial stage of the present study, the interaction mechanism between the studied ILs and sulfur compounds was studied. The study was performed based on 1-butyl-3-methylimidazolium octylsulfate, [bmim][OSO_4] where the desulfurization performance, K_d values were obtained from the literatures, in which seven type of sulfur compounds were tested experimentally (*Eßer et al. 2004*). In this study, the predictions performance were estimated based on performance index (PI) from COSMO-RS calculation via activity coefficient at infinite dilution, as shown in Table 4.1. Both K_d and PI values describe the extractability of ILs toward sulfur compounds from oil phase. Both literatures and predicted data are illustrated in Figure 4.1 for comparison purposes.

As presented in Figure 4.1, the K_d values of [bmim][OSO_4] for the seven type of sulfur compounds follow the order DBT > BT > 4-MDBT > 4,6-DMDBT > thiophene > tetrahydrothiophene > dodecanethiol; while the PI values gave a different order, which is thiophene > tetrahydrothiophene > BT > DBT > 4-MDBT > 4,6-DMDBT > dodecanethiol. A similar order was also observed using different ILs, 1-(4-sulfonic

acid) butyl-3-methylimidazolium *p*-toluenesulfonate (*Liu[b] et al. 2008*) and 1-ethyl-3-methylimidazolium diethylphosphate (*Nie et al. 2006*), respectively. The differences between PI and K_d values is due to the different basis used for the interaction mechanism calculation, where PI value is predicted mainly from hydrogen bonding while the observed interaction mechanism involved between ILs and sulfur compounds is through π-π interaction, from which K_d value is calculated.

In the application of ILs, most researchers described that the extractability of ILs toward sulfur compounds particularly relies on the electron-π density of the sulfur compounds (*Liu[b] et al. 2008*). Here in the case of [bmim][OSO_4], the formation of liquid clathrates and π-π interaction between sulfur compounds and the imidazolium ring of [bmim][OSO_4] indicates of possible interaction that exist during extractive desulfurization process (*Eβer et al. 2004; Liu[b] et al. 2008*). Therefore, this interaction mechanism needs to be investigated, and this information can be used for the development of new prediction method. This approach can be used to complement the COSMO-RS method so as to generate more reliable prediction.

Table 4.1: The activity coefficient (Act. Coeff.) at infinite dilution determined from the COSMO-RS software, calculated selectivity (Sel.), capacity (Cap.) and performance index (PI)

Compound	Act.Coeff.	Sel.	Cap.	PI
Dodecanethiol	14.897	3.744	0.067	0.251
Tetrahydrothiophene	1.075	51.897	0.930	48.284
Thiophene	0.904	61.673	1.106	68.190
Benzothiophene (BT)	1.486	37.537	0.673	25.261
Dibenzothiophene (DBT)	2.504	20.178	0.362	7.300
4-methyldibenzothiophene (4-MDBT)	3.657	15.254	0.273	4.171
4,6-dimethyldibenzothiophene (4,6-DMDBT)	4.955	11.257	0.202	2.272
n-dodecane	55.779			

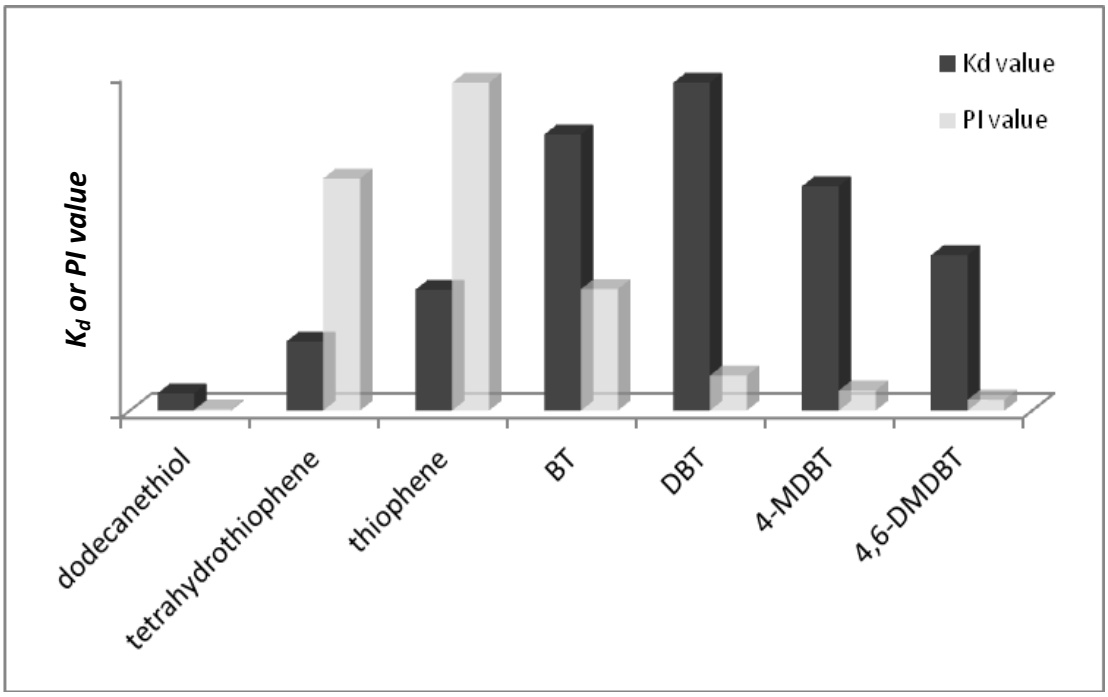

Figure 4.1: Extractability variations of the sulfur compounds using [bmim][OSO_4] for collected (*Eβer et al. 2004*) and predicted data

On the other hand, as for the prediction data calculated based on COSMO-RS, the explanations came from the sigma profile plot, as shown in Figure4.2. On the left hand side of the histogram is the hydrogen bond donor region ($\sigma < -\sigma_{HB}$; $\sigma_{HB} \sim 0.009$ e/Å^2) and on the right hand side is the hydrogen acceptor region ($\sigma > \sigma_{HB}$; $\sigma_{HB} \sim 0.009$ e/Å^2) (*Eckert and Klamt, 2002*). From the figure, it can be seen that the cation, [$bmim^+$] lies in the donor region while the anion, [OSO_4^-] lies in the acceptor region. A small fraction of the sigma profile of sulfur compounds stretched out into the donor and acceptor region, thus indicating that the sulfur compounds favour a very weak hydrogen bonding. The overlapping of the sigma profile between the sulfur compounds and [bmim][OSO_4] represents that miscibility between these compounds is possible. However, thiophene showed more overlaps compared to the other sulfur compounds which proves that more thiophene will be extracted from *n*-C_{12} as per estimation. These inconsistent observations between collected data (K_d value) and predicted data from COSMO-RS neccesitated the use of a third method; in this work we decided to investigate the interaction mechanism between BT molecules and [bmim][OSO_4] using Raman spectroscopy.

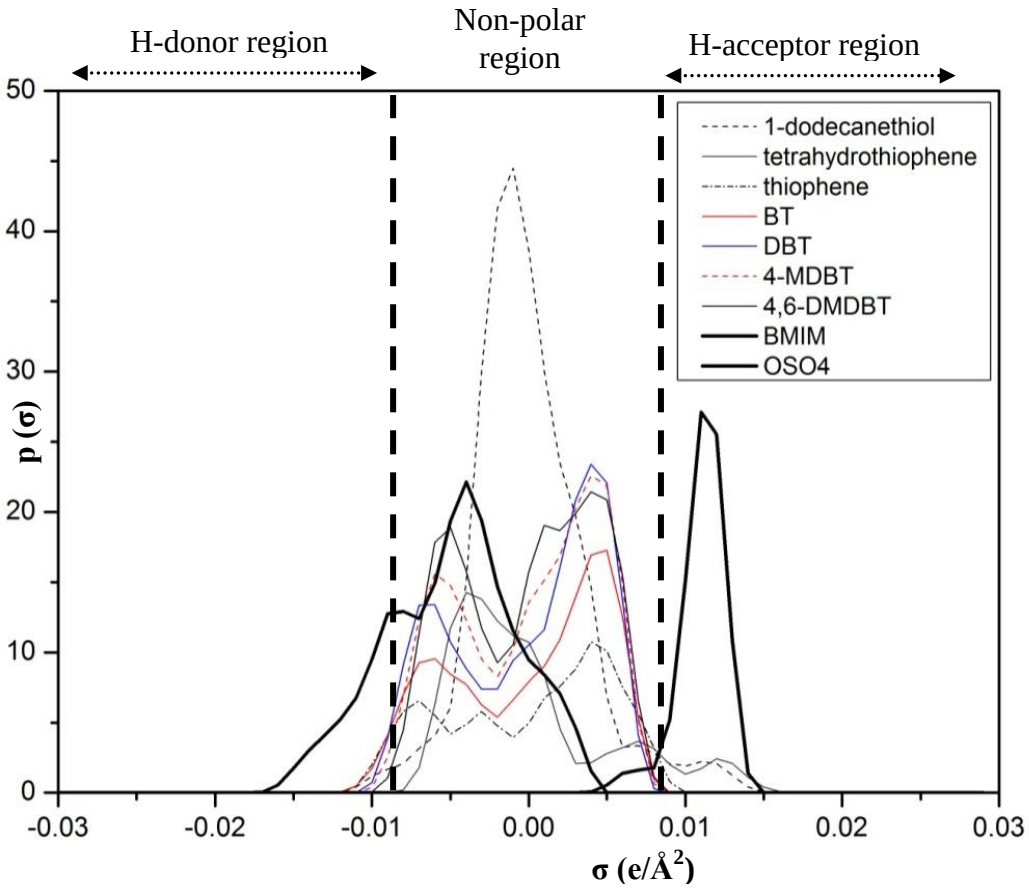

Figure 4.2: Sigma profile for [bmim][OSO_4] and respective sulfur species

4.2 Interaction Mechanism Study between [bmim][OSO_4] and BT using Raman Spectrocopy

Raman spectroscopy is a vibrational molecular spectroscopy which derives from an inelastic light scattering process. In Raman spectroscopy, sample preparation is simpler as compared to other Fourier transforms spectroscopy techniques. Basically with Raman spectroscopy, a laser photon is scattered by a sample molecule which loses or gains energy during the process. The amount of energy lost is seen as a change in energy (wavelength) of the irradiating photon. This energy loss is characteristics for a particular bond in the molecule. Figure 4.3 and 4.4 show the comparison of a Raman spectra where shifting occurred for two identified peaks at 1560 and 1420 cm^{-1}, respectively. By observing these peaks, the shifted peaks have

been assigned to C=C stretching at 1560 cm^{-1} and C-H vibration at 1420 cm^{-1} of the aromatic ring system. It is probable that the interaction largely involved the π-bond of BT and the C-H at imidazolium cation of [bmim][OSO_4]. With respect to this finding, it seems the aromaticity effect is the dominant factor influencing the trend of peak shifting in the Raman spectra for both BT and [$bmim^+$].

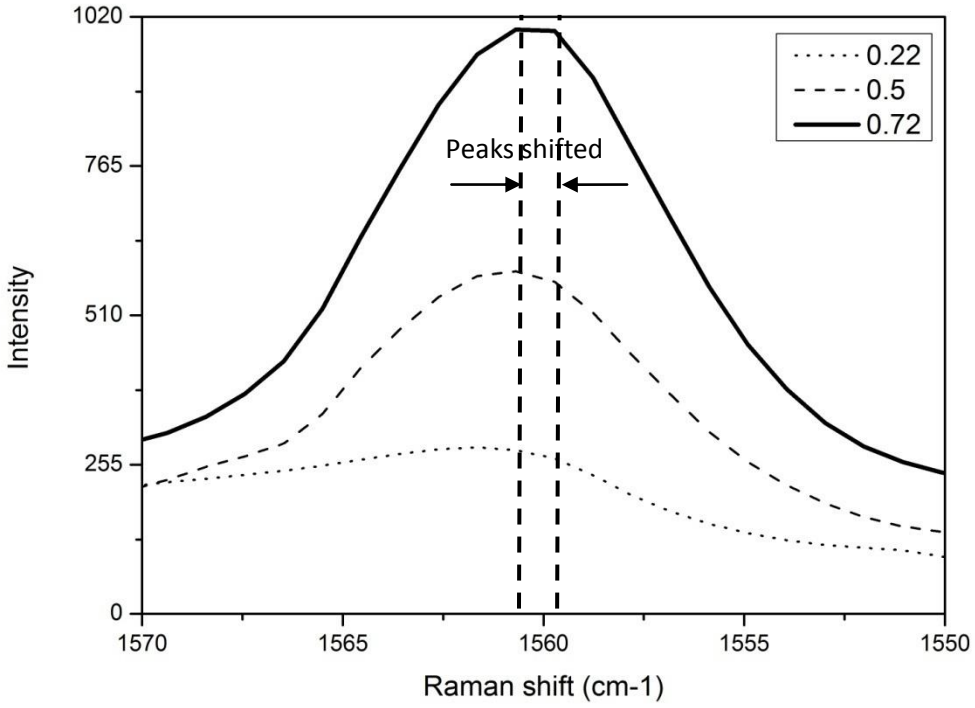

Figure 4.3: Raman spectra of {*x* BT + (1-*x*) [bmim][OSO_4]} over the range of 1570 – 1550cm^{-1} with the mole fraction increases from 0.22 to 0.72 BT

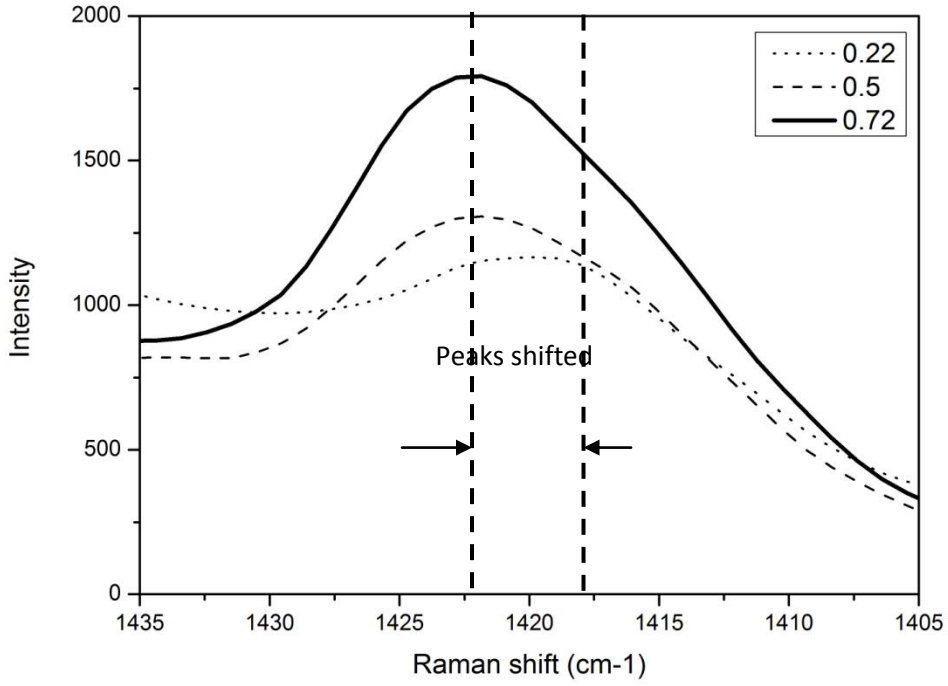

Figure 4.4: Raman spectra of {*x* BT + (1-*x*) [bmim][OSO_4]} over the range of (b) 1435 – 1405cm^{-1} with the mole fraction increases from 0.22 to 0.72 BT

As being discussed earlier, it proved that aromaticity effect played a crucial role in extracting aromatic sulfur compound which assisted the conceptual observation that majorly explicated by the hydrogen bonding of COSMO-RS. Other study indicated that, strong aromatic ring interaction occurred between thiophene and [$bmim^+$], based on NMR spectroscopy study (*Su et al. 2004*). This mechanism may support qualitatively that [bmim][OSO_4] can extract any aromatic sulfur compounds. However, more qualitative approach to predict the performance of ILs is required. Instead of relying on π-electron density, AI and DBE calculation will be performed to predict the potential ILs for diesel desulfurization quantitatively. But first, pre-assessment are needed in order to justify this screening method.

4.3 Selection of Potential ILs for Extractive Desulfurization

The AI of five aromatic sulfur compounds (TS, BT, DBT, 4-MDBT, 4,6-DMDBT) was calculated using Eq. 3.4 and the results are illustrated in Figure 4.5. With the aim of looking for some pattern within each aromatic sulfur compound, the information in

the figure has been added with data gathered from the literatures. The AI value of five studied compounds were found to be relatively proportional with the collected data whereby they followed the order of DBT > BT > TS > 4-MDBT > 4,6-DMDBT. Apart from considering the molecular size or alkyl chain length, whereby the performance on extractive desulfurization linearly increases with an increase of the alkyl chain length (*Nie et al. 2008; Mochizuki and Sugawara, 2008*), there is an alternative explanation to describe the miscibility of aromatic sulfur compounds in imidazolium-based ILs; miscibility decreases as the calculated AI value decreases. This fact indicates that calculating AI value could become a prediction tool for miscibility study of aromatic compounds in imidazolium-based ILs. Due to this, it is particularly exciting that the relationship between AI values and the experimental data of aromatic sulfur compounds may open the possibility for screening potential ILs for the desulfurization process.

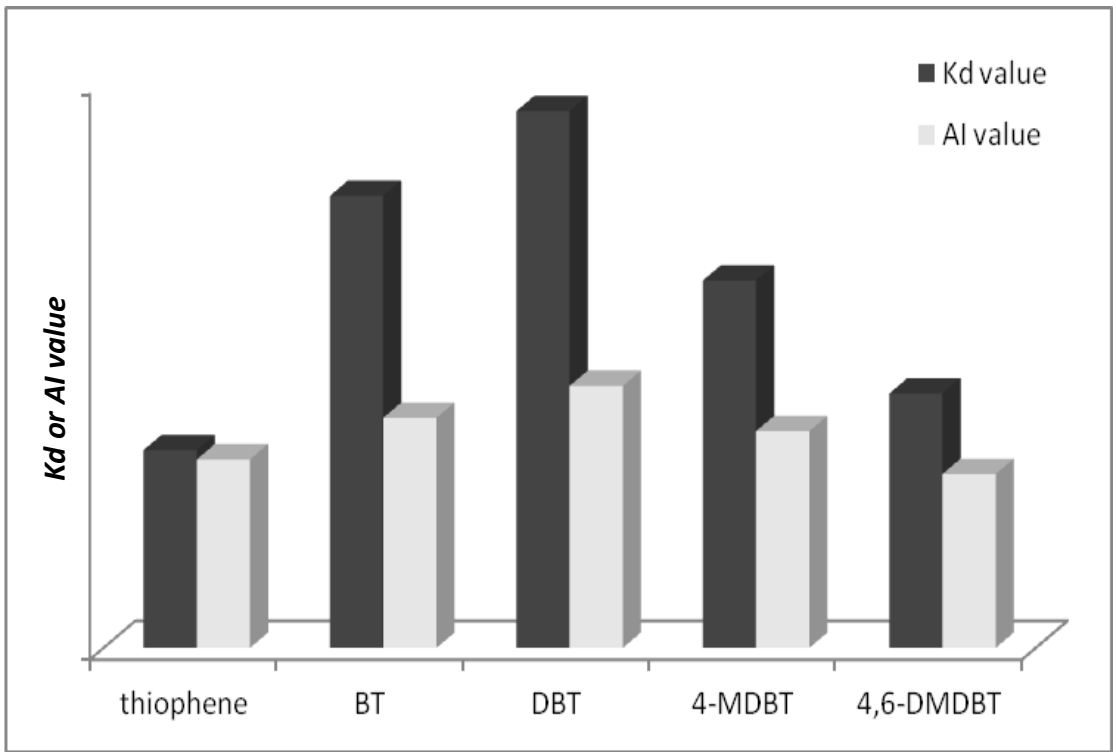

Figure 4.5: Comparison of extractability (K_d value) aromatic sulfur compounds collected from literature (*Eβer et al. 2004*) and AI value

Table 4.2 shows the calculated AI and DBE values for common cation and anion, respectively. From the table, a combination of 11 cations and 37 anions, which resulted in 407 possible ILs, are screened to obtain the best IL for removal of sulfur compounds from diesel.

The AI values were calculated based on the root structure of cation alone and the attached alkyl chain was ignored prior in justifying the pattern towards experimental result of extractive desulfurization (K_d value). Besides weakening the Coulombic interaction between anion and cation of ILs, the alkyl chain attached to the root structure of cation are not favourable in π-π interaction between ILs and sulfur compounds. Therefore, only root structure is considered for AI calculation.

For anion, DBE value was investigated instead of AI due to the limited number of current available anions. Same principle was applied for calculating DBE value where root structure is counted for valued. From 407 possible ILs, 25 ILs are identified to synthesize and characterize for further investigation and validation (which discussed in Chapter 5). Five ILs are proposed for cation validation and another 20 ILs for anion, which are tabulated in Table 4.3.

Table 4.2: Calculated aromaticity index (AI) and double-bond equivalent (DBE) value for common cation and anion

Cation (basic structure)		Anion	
Chemical formula	**AI**	**Chemical formula**	**DBE**
Benzimidazole, $C_7H_6N_2$	1	Acetate, $C_2H_3O_2$	1.5
Benzyltriphenylphosphine, $C_{25}H_{21}P$	0.6458	Benzoate, $C_7H_5O_2$	5.5
		Bis(tpM)phos., $C_{16}H_{34}O_2P$	0.5
Guanidine, CH_5N_3	-	Butylsulfate, $C_4H_9O_4S$	0.5
Imidazole, $C_3H_4N_2$	2	Decanoate, $C_{10}H_{19}O_2$	1.5
Oxazole, C_3H_3NO	1.5	DBP, $C_8H_{18}O_4P$	0.5
Piperidine, $C_4H_{10}N_2$	0	Dicyanamide, C_2N_3	4.5
Pyrazole, $C_3H_4N_2$	2	DEP, $C_4H_{10}O_4P$	0.5
Pyridine, C_5H_5N	0.875	DHP, H_2O_4P	0.5
Pyrrolidine, C_4H_9N	-	DMP, $C_2H_6O_4P$	0.5
Quinoline, C_9H_7N	1.083	$EESO_4$, $C_4H_9O_5S$	0.5
Thiazole, C_3H_3NS	1.5	ESO_4, $C_2H_5O_4S$	0.5
		Hydrogensulfate, HSO_4	0.5
		Methanesulfonate, CH_3O_3S	0.5
		$MESO_4$, $C_3H_7O_5S$	0.5
		MSO_4, CH_3O_4S	0.5
		Nitrate, NO_3	1.5
		OSO_4, $C_8H_{17}O_4S$	0.5
		Salicylate, $C_7H_5O_3$	5.5
		Thiocyanate, CNS	2.5
		TOS, $C_7H_7O_3S$	4.5
		TCM, C_4N_3	6.5
		$(ME)ESO_4$, $C_5H_{11}O_6S$	0.5
		Imidazolide or pyrazolide, $C_3H_3N_2$	3.5
		Bis(PFE)phos., $C_4F_{10}O_2P$	0.5
		Bis(PFES)ami., $C_4F_{10}NO_4S_2$	0.5
		Bis(TFM)imi., C_2F_6N	0.5
		Bis(TFMS)meth., $C_3HF_6O_4S_2$	0.5
		Perchlorate, ClO_4	0.5
		HFB, $C_4F_7O_2$	0.5
		IOPF, $F_4NO_2P_2$	0.5
		pFBS, $C_4F_9O_3S$	0.5
		NTf_2, $C_2F_6NO_4S_2$	0.5
		TFA, $C_2F_3O_2$	1.5
		OTf, CF_3O_3S	0.5
		Tris(tFMS)meth., $C_4F_9O_6S_3$	0.5

Table 4.3: Selected 25 ILs with their respective calculated AI and DBE values

Cation	AI value	Anion	DBE value	Physical state at room temperature
1,3-dimethylimidazolium	2	MSO_4	0.5	Liquid
1,2-dimethylpyrazolium	2	MSO_4	0.5	Liquid
1,3-dimethylbenzimidazolium	1	MSO_4	0.5	Solid
1,4-dimethylpyridinium	0.875	MSO_4	0.5	Liquid
1,1-dimethylpyrrolidinium	0	MSO_4	0.5	Liquid
1-butyl-3-methylimidazolium	2	DHP	0.5	Liquid
1-butyl-3-methylimidazolium	2	DMP	0.5	Liquid
1-butyl-3-methylimidazolium	2	DBP	0.5	Liquid
1-butyl-3-methylimidazolium	2	HSO_4	0.5	Liquid
1-butyl-3-methylimidazolium	2	MSO_4	0.5	Liquid
1-butyl-3-methylimidazolium	2	BSO_4	0.5	Liquid
1-butyl-3-methylimidazolium	2	OSO_4	0.5	Liquid
1-butyl-3-methylimidazolium	2	OTf	0.5	Liquid
1-butyl-3-methylimidazolium	2	NTf_2	0.5	Liquid
1-butyl-3-methylimidazolium	2	Acetate	1.5	Liquid
1-butyl-3-methylimidazolium	2	TFA	1.5	Liquid
1-butyl-3-methylimidazolium	2	NO_3	1.5	Liquid
1-butyl-3-methylimidazolium	2	CNS	2.5	Liquid
1-butyl-3-methylimidazolium	2	Imidazolide	3.5	Liquid
1-butyl-3-methylimidazolium	2	Pyrazolide	3.5	Liquid
1-butyl-3-methylimidazolium	2	TOS	4.5	Solid
1-butyl-3-methylimidazolium	2	Dicyanamide	4.5	Liquid
1-butyl-3-methylimidazolium	2	Benzoate	5.5	Liquid
1-butyl-3-methylimidazolium	2	Salicylate	5.5	Liquid
1-butyl-3-methylimidazolium	2	TCM	6.5	Liquid

4.4 Characterization of Potential ILs

As discussed previously in the selection of ILs for extractive desulfurization process, the desulfurization ability of 25 potential ILs towards BT in *n*-C_{12} was carried out. Out of the 25 potential ILs, 13 were synthesized in-house while another 12 were purchased from Merck. Their characterization were conducted accordingly. Structural and elemental composition analysis were conducted only for synthesized ILs.

4.4.1 Structural, Elemental Composition, Water and Halide Content Evaluation

The structure of each synthesized ILs was identified by ^{1}H NMR accordingly. ILs within the same root of anion, but has different alkyl chain length were additionally identified by ^{13}C NMR. The elemental composition, water and halide content were also studied and their results are as follows:

1,3-dimethylimidazolium methylsulfate, [mmim][MSO_4]

Yield: 86% (4.3g) as pale yellow liquid, ^{1}H NMR (500 MHz, D_2O, ppm): 8.07 [t, 1H(im)], 7.93 [d, 1H(im)], 6.57 [d, 1H(im)], 3.66 [s, 3H, OCH_3], 3.23 [s, 6H, NCH_3]. Elemental analysis, % found (% calculated): C, 34.97 (34.61), H, 5.45 (5.81), N, 13.80 (13.45), S, 15.38 (15.40).

1,2-dimethylpyrazolium methylsulfate, [mmpyz][MSO_4]

Yield: 87% (6.1g) as pale yellow liquid, ^{1}H NMR (500 MHz, D_2O, ppm): 8.02 [t, 1H(pyz)], 7.91 [d, 1H(pyz)], 6.55 [d, 1H(pyz)], 3.97 [s, 3H, OCH_3], 3.88 [s, 3H, NCH_3], 3.49 [s, 3H, CH_3]. Elemental analysis, % found (% calculated): C, 34.21 (34.61), H, 5.97 (5.81), N, 13.39 (13.45), S, 15.58 (15.40).

1,3-dimethylbenzimidazolium methylsulfate, [mmBzim][MSO_4]

Yield: 87% (5.4g) as white powder salt, ^{1}H NMR (500 MHz, D_2O, ppm): 9.13 [s, 1H(bzim)], 7.77 [d, 1H(bzim)], 7.58 [d, 1H(bzim)], 4.41 [d, 1H(bzim)], 3.98 [d, 1H(bzim)], 3.62 [s, 3H, OCH_3], 1.49 [t, 3H, CH_3], 1.18 [t, 3H, CH_3]. Elemental analysis, % found (% calculated):C, 45.97 (46.50), H, 4.76 (5.46), N, 10.12 (10.85), S, 11.85 (12.42).

1,4-dimethylpyridinium methylsulfate, [mmpy][MSO_4]

Yield: 88% (5.2g) as yellowish liquid, ^{1}H NMR (500 MHz, D_2O, ppm):8.63 [d, 1H(py)], 8.39 [t, 2H(py)], 7.90 [t, 1H(py)], 4.74 [s, 3H, OCH_3], 4.25 [s, 3H, NCH_3], 3.55 [s, 3H, CH_3]. Elemental analysis, % found (% calculated): C, 44.33 (44.03), H, 5.34 (5.54), N, 6.77 (6.42), S, 15.05 (14.69).

1,1-dimethylpyrrolidinium methylsulfate, [mmpyrr][MSO_4]

Yield: 88% (4.4g) as yellowish viscous liquid, ^{1}H NMR (500 MHz, D_2O, ppm): 8.03 [t, 4H(pyrr)], 7.57 [t, 4H(pyrr)], 3.97 [s, 3H, OCH_3], 3.95 [s, 6H, NCH_3]. Elemental analysis, % found (% calculated): C, 40.15 (39.80), H, 7.78 (8.11), N, 6.56 (6.63), S, 14.81 (15.18).

1-butyl-3-methylimidazolium dihydrogenphosphate, [bmim][DHP]

Yield: 67% as colorless liquid, ^{1}H NMR (500 MHz, D_2O, ppm): 8.51 [s, 1H(im)], 7.34 [d, 1H(im)], 7.29 [d, 1H(im)], 4.07 [t, 2H, CH_2], 3.76 [s, 3H, CH_3], 2.64 [s, 1H, OH], 2.18 [s, 1H, OH], 1.73-1.69 [m, 2H, CH_2], 1.19-1.16 [m, 2H, CH_2], 0.80 [t, 3H, CH_3]. ^{13}C NMR (500 MHz, D_2O, ppm): 135.11 [s, 1C], 123.41 [d, 1C], 122.16 [d, 1C], 49.24 [d, 1C], 35.56 [s, 1C], 31.22 [d, 1C], 18.72 [d, 1C], 12.59 [d, 1C]. Elemental analysis, % found (% calculated): C, 41.01 (40.68), H, 7.03 (7.25), N, 12.17 (11.86).

1-butyl-3-methylimidazolium dimethylphosphate, [bmim][DMP]

Yield: 91% (5.8g) as yellowish liquid, ^{1}H NMR (500 MHz, D_2O, ppm): 8.58 [s, 1H(im)], 7.36 [d, 1H(im)], 7.31 [d, 1H(im)], 4.08 [t,2H, CH_2], 3.76 [s, 3H, CH_3], 3.47 [s, 3H, CH_3], 3.45 [s, 3H, CH_3], 1.73-1.68 [m, 2H, CH_2], 1.20-1.16 [m, 2H, CH_2], 0.79 [t, 3H, CH_3]. ^{13}C NMR (500 MHz, D_2O, ppm): 135.08 [s, 1C], 122.42 [d, 1C], 122.30 [d, 1C], 66.02 [d, 1C], 65.98 [d, 1C], 49.28 [s, 1C], 31.98 [t, 1C], 31.54 [t, 1C], 31.22 [t, 1C], 18.73 [t, 1C], 18.35 [t, 1C], 12.99 [t, 1C], 12.75 [d, 1C], 12.58 [d, 1C]. Elemental analysis, % found (% calculated): C, 44.39 (45.43), H, 8.11 (8.89), N, 10.85 (10.61).

1-butyl-3-methylimidazolium dibutylphosphate, [bmim][DBP]

Yield: 93% (7.8g) as pale yellow liquid, ^{1}H NMR (500 MHz, D_2O, ppm): 8.66 [s, 1H(im)], 7.36 [d, 1H(im)], 7.34 [d, 1H(im)], 4.08 [t, 2H, CH_2], 4.07 [t, 2H, CH_2], 4.05 [t, 2H, CH_2], 3.74 [s, 3H, CH_3], 1.73-170 [m, 2H, CH_2], 1.70-1.68 [m, 2H, CH_2], 1.49-1.46 [m, 2H, CH_2], 1.27-1.23 [m, 2H, CH_2], 1.23-1.20 [m, 2H, CH_2], 1.18-1.14 [m, 2H, CH_2], 0.80 [t, 3H, CH_3], 0.79 [t, 3H, CH_3], 0.78 [t, 3H, CH_3]. ^{13}C NMR (500 MHz, D_2O, ppm): 135.08 [s, 1C], 122.51 [d, 1C], 122.30 [d, 1C], 66.17 [d, 1C], 66.02 [d, 1C], 65.98 [d, 1C], 49.28 [s, 1C], 31.98 [t, 1C], 31.54 [t, 1C], 31.22 [t, 1C], 18.73 [t, 1C], 18.35 [t, 1C], 18.09 [t, 1C], 12.99 [d, 1C], 12.75 [d, 1C], 12.58 [d, 1C]. Elemental analysis, % found (% calculated): C, 54.98 (55.16), H, 9.76 (9.55), N, 8.14 (8.04).

1-butyl-3-methylimidazolium butylsulfate, [bmim][BSO_4]

Yield: 88% (6.2g) as pale yellow liquid, ^{1}H NMR (500 MHz, D_2O, ppm): 8.56 [s, 1H(im)], 7.39 [d, 2H(im)], 4.09 [t, 2H, OCH_2], 3.74 [s, 3H, $OC_3H_6CH_3$], 1.77-171 [m, 2H, CH_2], 1.56-1.50 [m, 2H, CH_2], 1.31-1.24 [m, 2H, CH_2], 1.22-1.16 [m, 2H, CH_2], 0.80 [t, 3H, CH_3], 0.79 [t, 3H, CH_3].Elemental analysis, % found (% calculated): C, 50.33 (51.06), H, 5.16 (5.00), N, 10.11 (9.92), S, 11.12 (11.36).

1-butyl-3-methylimidazolium imidazolide, [bmim][Imd]

Yield: 72% as brownish liquid, ^{1}H NMR (500 MHz, D_2O, ppm): 8.43 [s, 1H(imd)], 7.72 [s, 1H(im)], 7.41 [d, 1H(imd)], 7.37 [d, 1H(imd)], 7.09 [d, 2H(im)], 4.13 [t, 2H, NCH_2], 3.66 [s, 3H, NCH_3], 1.82-1.76 [m, 2H, CH_2], 1.29-1.25 [m, 2H, CH_2], 0.88 [t, 3H, CH_3]. Elemental analysis, % found (% calculated): C, 63.78 (64.05), H, 8.81 (8.79), N, 26.77 (27.16).

1-butyl-3-methylimidazolium pyrazolide, [bmim][Pyd]

Yield: 71% as yellowish liquid, ^{1}H NMR (500 MHz, D_2O, ppm): 8.77 [s, 1H(im)], 7.98 [t, 1H(pyd)], 7.68 [d, 1H(pyd)], 7.61 [d, 1H(pyd)], 6.35 [d, 2H(im)], 4.25 [t, 2H, CH_2], 3.96 [s, 3H, CH_3], 1.93-1.85 [m, 2H, CH_2], 1.44-1.34 [m, 2H, CH_2], 0.99 [t, 3H, CH_3]. Elemental analysis, % found (% calculated): C, 64.38 (64.05), H, 8.98 (8.79), N, 27.45 (27.16).

1-butyl-3-methylimidazolium benzoate, [bmim][BZT]

Yield: 81% (10.5g) as yellowish liquid, ^{1}H NMR (500 MHz, D_2O, ppm): 8.51 [d, 1H(bzt)], 7.76 [d, 1H(bzt)], 7.43 [d, 1H(bzt)], 7.37 [s, 1H(im)], 7.35 [d, 2H(im)], 7.29 [d, 1H(bzt)], 7.25 [d, 1H(bzt)], 4.00 [t, 2H, CH_2], 3.71 [s, 3H, CH_3], 1.70-1.64 [m, 2H, CH_2], 1.18-1.12 [m, 2H, CH_2],0.78 [t, 3H, CH_3]. Elemental analysis, % found (% calculated): C, 68.55 (69.20), H, 8.09 (7.74), N, 11.05 (10.76).

1-butyl-3-methylimidazolium salicylate, [bmim][SCL]

Yield: 65% as light brown liquid, ^{1}H NMR (500 MHz, D_2O, ppm): 8.25 [s, 1H(im)], 7.55 [t, 1H(scl)], 7.14 [t, 1H(scl)], 7.06 [d, 2H(im)], 6.63 [d, 2H(scl)], 3.76 [t, 2H, CH_2], 3.58 [s, 3H, CH_3], 1.50-1.42 [m, 2H, CH_2], 1.05-0.95 [m, 2H, CH_2], 0.67 [t, 3H, CH_3].Elemental analysis, % found (% calculated): C, 65.11 (65.20), H, 7.23 (7.30), N, 10.27 (10.14).

Before conducting extractive desulfurization process, structural and elemental analysis data need to be confirmed first, and water and halide content of ILs should be determined to ensure that they are within the acceptable limit. In this study, the gazetted acceptable limit is less than 500 ppm for both water and halide content; these limits are applied for all 25 ILs due to their effect in desulfurization performance. In general, by referring to the above data, most of the synthesized ILs through alkylation contained less water and halide as compared to ILs produced via metathesis and neutralization, merely due to the synthesized routes of ILs itself. For purchased ILs, the water and halide content were already stated, but they were inaccurate, therefore the water and halide contents were repeated in the laboratory prior using them for extractive desulfurization and their results are as follows. Both water and halide content were tabulated in Table 4.4.

Table 4.4: List of potential ILs with their respective water and halide content

Name of ILs	Acronym	Water content (ppm)	Halide content (ppm)
1,3-dimethylimidazolium methylsulfate	[mmim][MSO_4]	284	45
1,2-dimethylpyrazolium methylsulfate	[mmpyz][MSO_4]	223	42
1,3-dimethylbenzimidazolium methylsulfate	[mmBzim][MSO_4]	327	63
1,4-dimethylpyridinium methylsulfate	[mmpy][MSO_4]	172	53
1,1-dimethylpyrrolidinium methylsulfate	[mmpyrr][MSO_4]	274	76
1-butyl-3-methylimidazolium dihydrogenphosphate	[bmim][DHP]	456	411
1-butyl-3-methylimidazolium dimethylphosphate	[bmim][DMP]	286	123
1-butyl-3-methylimidazolium dibutylphosphate	[bmim][DBP]	384	128
1-butyl-3-methylimidazolium hydrogensulfate	[bmim][HSO_4]	154	104
1-butyl-3-methylimidazolium methylsulfate	[bmim][MSO_4]	197	63
1-butyl-3-methylimidazolium butylsulfate	[bmim][BSO_4]	211	129
1-butyl-3-methylimidazolium octylsulfate	[bmim][OSO_4]	231	84
1-butyl-3-methylimidazolium trifluoromethanesulfonate	[bmim][OTf]	173	92
1-butyl-3-methylimidazolium bis(trifluoromethanesulfonyl)imide	[bmim][NTf_2]	164	103
1-butyl-3-methylimidazolium acetate	[bmim][Ac]	204	115
1-butyl-3-methylimidazolium trifluoroacetate	[bmim][TFA]	181	121
1-butyl-3-methylimidazolium nitrate	[bmim][NO_3]	161	78
1-butyl-3-methylimidazolium thiocyanate	[bmim][CNS]	155	82
1-butyl-3-methylimidazolium imidazolide	[bmim][Imd]	459	394
1-butyl-3-methylimidazolium pyrazolide	[bmim][Pyd]	471	443
1-butyl-3-methylimidazolium tosylate	[bmim][TOS]	251	102
1-butyl-3-methylimidazolium dicyanamide	[bmim][DCA]	215	118
1-butyl-3-methylimidazolium benzoate	[bmim][BZT]	361	404
1-butyl-3-methylimidazolium salicylate	[bmim][SCL]	374	403
1-butyl-3-methylimidazolium tricyanomethane	[bmim][TCM]	167	61

4.4.2 Physical Properties Evaluation

The physical properties (density and refractive index) of the 25 ILs were determined using Anton Paar DMA 5000M and ATAGO RX-5000 Alpha, respectively. For this study, these properties are essential for investigating the behaviour of potential ILs. These investigations are needed for further utilization of ILs in commercial applications such as for designing and scaling-up of process equipment.

4.4.2.1 Density Analysis

Density is an important property for purity evaluation. The density of ILs falls typically in the range of 0.9 – 1.30 $g.cm^{-3}$. Figure 4.6 shows the temperature dependence of density for four selected sulfate-based ILs. [bmim][HSO_4] has a higher density than other sulfate-based ILs. This shows that higher density liquids have a lesser alkyl chain length. In [bmim][HSO_4], the Coulombic attraction between cation and anion interacts more closely with each other, which tightens the [$bmim^+$] and [HSO_4^-] as a molecule, hence attributes to the higher density. Likewise, decreasing of the alkyl chain length, from octyl to methyl showed increasing density from 1.0606 to 1.2958$g.cm^{-3}$. This observation is similar to that observed in phosphate-based ILs where [bmim][DHP] has the highest density, as shown in Figure 4.7. The values of all 23 ILs are tabulated in the Appendix C (Figure C1 – C8) accordingly.

As can be seen in two figures (Figure 4.6 and 4.7), temperature and density show a linear correlation of more than 99.5%. Thus, the linear equation can be used for calculating the density of any of the 23 ILs at temperatures in the range of 298.15 to 348.15 K. The densities of [bmim][MSO_4] and [bmim][OSO_4] are in good agreement with those reported by Tariq et *al*. (2009) and Wasserscheid et *al.* (2002), respectively. Characterization of the two ILs namely [mmBzim][MSO_4] and [bmim][TOS] were not attempted due to their existence in solid state form.

The values of the density, ρ were fitted using the following form of linear equation (*Pereiro et al. 2007*):

$$\rho = A_0 + A_1 T \tag{4.1}$$

where ρ is the density, T is the temperature, and A_0 and A_1 are correlation coefficients established using the method of least squares. The estimated correlation coefficients and standard deviations, *SD* are presented in Table 4.5. The *SD* were calculated using the following equation:

$$SD = \sqrt{\frac{\sum_i^{n_{DAT}} \left(Z_{Expt} - Z_{Calc}\right)^2}{n_{DAT}}} \tag{4.2}$$

where n_{DAT} is the number of experimental points and Z_{Expt} and Z_{Calc} are experimental and calculated values, respectively.

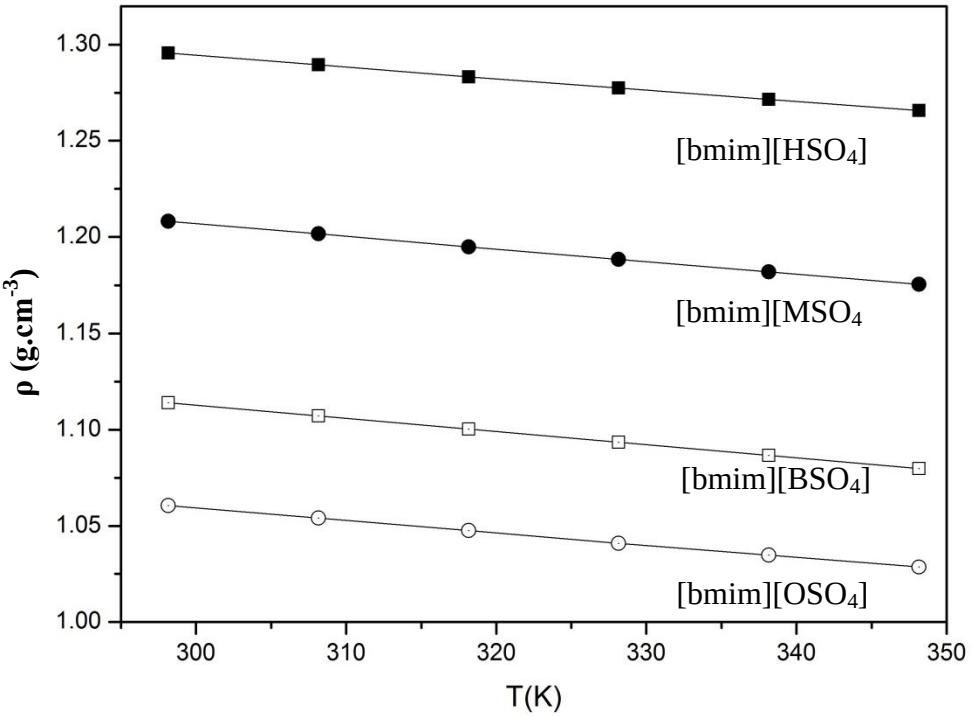

Figure 4.6: Density of sulfate-based ILs at various temperatures

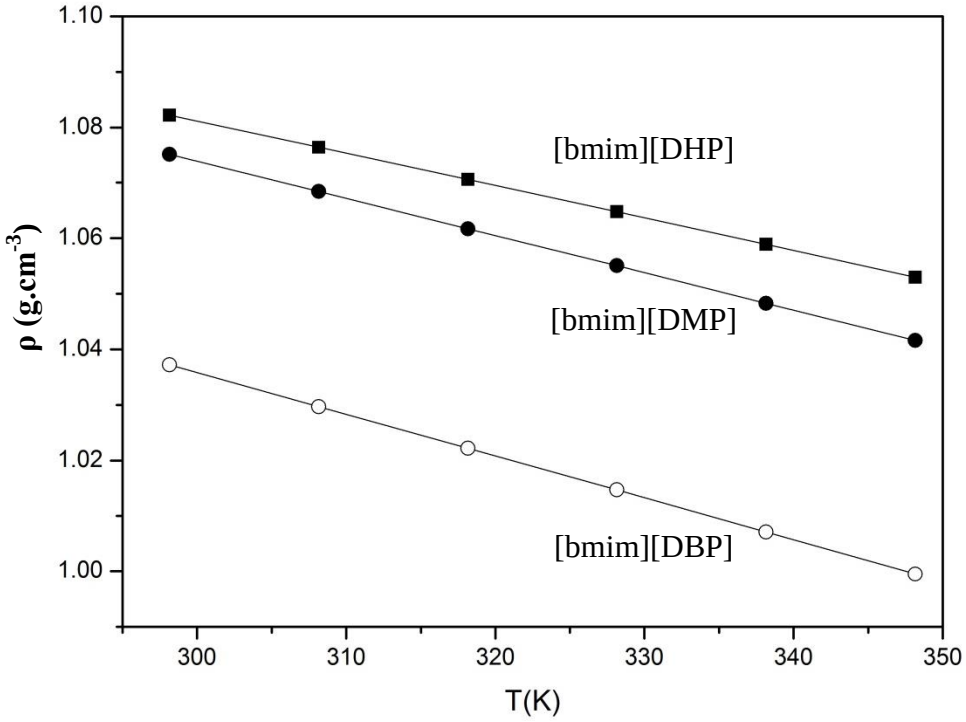

Figure 4.7: Density of phosphate-based ILs at various temperatures

The coefficient of thermal expansion can be derived from density as a function of temperature, whereby this coefficient is important in observing the changes of ILs sizes with a change in temperature. The coefficient of thermal expansion for the 23 ILs was calculated from the experimental density values using the following equation:

$$\alpha_p = 1/\rho \cdot \left(\partial\rho/\partial T\right)_p = \frac{-\left(A_1\right)}{\left(A_0 + A_1 T\right)} \tag{4.3}$$

where α_p is the coefficient of thermal expansion, and the definitions of ρ, T, A_0 and A_1, are as given previously for Eq. 4.1. The values of thermal expansion coefficients of the ILs are tabulated in Table 4.6. As can be observed, the coefficient of thermal expansion do not change appreciably, therefore these coefficient can be considered as independent of temperature, which are good agreement with those of imidazolium-based and pyridinium-based ILs (*Pereiro et al. 2007; Yunus et al. 2010*).

Table 4.5: Fitting parameters of Eq. 4.1 to correlate density of 23 ILs and standard deviation (*SD*) calculated using Eq. 4.2

Ionic Liquid (ILs)	$\mathbf{A_0}$	$\mathbf{A_1}$	$\mathbf{R^2}$	**SD**
[mmim][MSO_4]	1.5066	-0.0007	0.9999	0.0001
[mmpyz][MSO_4]	1.5919	-0.0007	0.9999	0.0103
[mmpy][MSO_4]	1.5966	-0.0006	0.9999	0.0069
[mmpyrr][MSO_4]	1.5223	-0.0007	0.9990	0.0060
[bmim][DHP]	1.2563	-0.0006	0.9999	0.0052
[bmim][DMP]	1.3434	-0.0007	0.9999	0.0113
[bmim][DBP]	1.2619	-0.0008	0.9999	0.0151
[bmim][HSO_4]	1.4750	-0.0006	0.9998	0.0005
[bmim][MSO_4]	1.4036	-0.0007	0.9999	0.0144
[bmim][BSO_4]	1.3167	-0.0007	0.9999	0.0065
[bmim][OSO_4]	1.2522	-0.0006	0.9999	0.0138
[bmim][OTf]	1.5275	-0.0008	0.9992	0.0078
[bmim][NTf_2]	1.6938	-0.0009	0.9999	0.0095
[bmim][Ac]	1.2305	-0.0006	0.9999	0.0011
[bmim][TFA]	1.4137	-0.0007	0.9999	0.0076
[bmim][NO_3]	1.3403	-0.0006	0.9999	0.0083
[bmim][CNS]	1.2437	-0.0006	0.9999	0.0058
[bmim][Imd]	1.3801	-0.0007	0.9920	0.0137
[bmim][Pyd]	1.3568	-0.0007	0.9999	0.0097
[bmim][DCA]	1.2439	-0.0006	0.9999	0.0076
[bmim][BZT]	1.2802	-0.0006	0.9999	0.0117
[bmim][SCL]	1.3454	-0.0007	0.9999	0.0160
[bmim][TCM]	1.2452	-0.0007	0.9999	0.0110

Table 4.6: Thermal expansion coefficients (α_p) of 23 ILs calculated using Eq. 4.3

T (K)	**$10^{-4}\alpha_p$ (K^{-1})**							
	[mmim] [MSO_4]	[mmp [MSO_4]	[mmpy] [MSO_4]	[mmPyrr] [MSO_4]	[bmim] [DHP]	[bmim] [DMP]	[bmim] [DBP]	[bmim] [HSO_4]
298.15	5.39	5.06	4.23	5.33	5.57	6.17	7.83	4.63
308.15	5.42	5.09	4.25	5.36	5.60	6.21	7.88	4.65
318.15	5.45	5.11	4.27	5.39	5.63	6.25	7.94	4.67
328.15	5.48	5.14	4.29	5.42	5.66	6.29	8.00	4.69
338.15	5.51	5.17	4.31	5.44	5.70	6.33	8.07	4.72
348.15	5.54	5.19	4.32	5.47	5.73	6.37	8.14	4.74
	[bmim] [MSO_4]	[bmim] [BSO_4]	[bmim] [OSO_4]	[bmim] [OTf]	[bmim] [NTf_2]	[bmim] [Ac]	[bmim] [TFA]	[bmim] [NO_3]
298.15	5.86	6.32	5.59	6.21	6.31	5.71	5.81	5.17
308.15	5.89	6.36	5.62	6.25	6.35	5.74	5.84	5.19
318.15	5.93	6.40	5.65	6.28	6.39	5.77	5.88	5.22
328.15	5.96	6.44	5.69	6.32	6.44	5.80	5.91	5.25
338.15	6.00	6.48	5.72	6.36	6.48	5.84	5.95	5.28
348.15	6.04	6.52	5.75	6.41	6.52	5.87	5.98	5.30
	[bmim] [CNS]	[bmim] Imd]	[bmim] [Pyd]	[bmim] [DCA]	[bmim] [BZT]	[bmim] [SCL]	[bmim] [TCM]	
298.15	5.63	5.98	6.10	5.63	5.45	6.16	6.75	
308.15	5.67	6.01	6.13	5.67	5.48	6.20	6.80	
318.15	5.70	6.05	6.17	5.70	5.51	6.23	6.85	
328.15	5.73	6.08	6.21	5.73	5.54	6.27	6.89	
338.15	5.76	6.12	6.25	5.76	5.57	6.31	6.94	
348.15	5.80	6.16	6.29	5.80	5.60	6.35	6.99	

4.4.2.2 Refractive Index Analysis

Refractive index of ILs is an important property for analysis as it indicates the compactness of ILs, where the higher its refractive index, the more tightly packed a compound is (*Deeflet et al. 2006*). A comparison of the experimental values of refractive index against literatures data shows a very satisfactory agreement as shown in Table 4.7. The minor differences in the values may be attributed to the difference in water and halide contents.

Table 4.7: Data used for the validation of equipment for refractive index, n_D measurement at T = 298.15 K

ILs	**Refractive index, n_D**	
	This work	**Literatures**
[bmim][MSO_4]	1.4712	1.4778 (*Tariq et al. 2009*)
[bmim][OTf]	1.4380	1.4366 (*Tariq et al. 2009*)
[bmim][NTf_2]	1.4263	1.4271 (*Huddleston et al. 2001*) 1.4285 (*Tariq et al. 2009*)

The refractive indices of all 23 ILs were measured and it was observed that all 23 ILs showed the same trend against temperature. Out of the 23 only four were selected for a more detailed study for temperature range presented in Figure 4.8. The measured refractive indices of these four ILs were observed to decrease linearly as the temperature increased. The refractive index also increases as the length of the alkyl chain of the anion increases, which is an opposite trend to that of the density. These observations could be attributed to the compactness effect of ILs molecules which is in good agreement with the literature findings (*Tariq et al. 2009; Yunus et al. 2010*). The values of refractive index for all 23 ILs are tabulated in the Appendix C (Figure C9 – C16) accordingly.

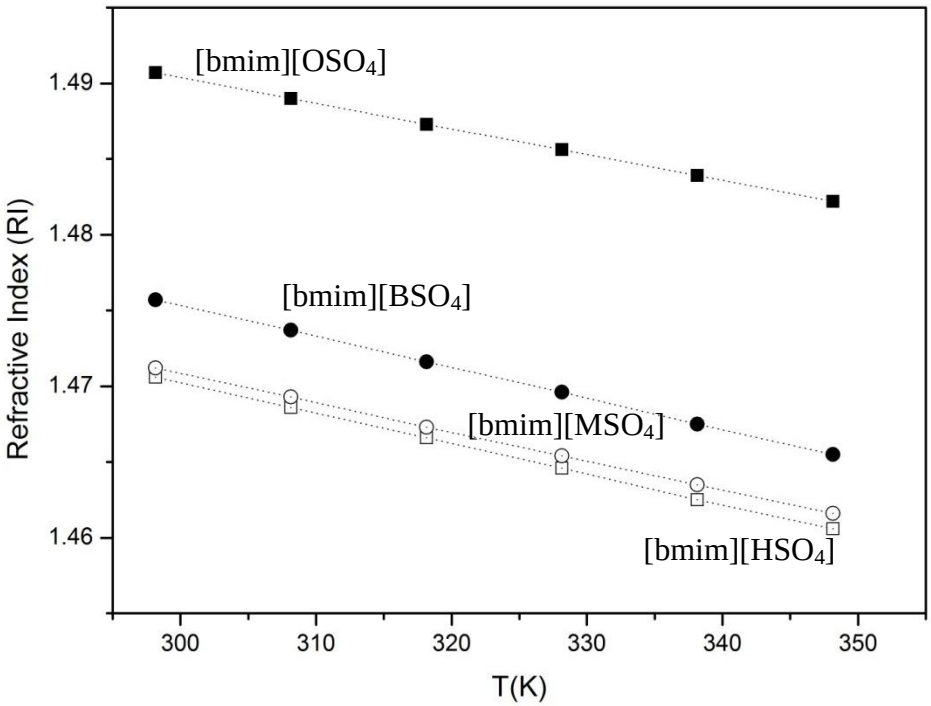

Figure 4.8: Plot of experimental refractive index of four sulfate-based ILs as a function of temperature, T = (298.15 – 348.15) K

The values of the refractive index, n_D were fitted using the following form of equation (*Pereiro et al. 2007*):

$$n_D = A_2 + A_3T \tag{4.4}$$

where n_D is the refractive index, T is the temperature in K, and A_2 and A_3 are correlation coefficients established using the method of least squares. The estimated correlation coefficients and standard deviations, *SD* are presented in Table 4.8 where *SD* was calculated using Eq. 4.2.

Table 4.8: Fitting parameters of Eq. 4.4 to correlate refractive index of 23 ILs and standard deviation (*SD*) calculated using Eq. 4.2

Ionic Liquid (ILs)	A_2	A_3	R^2	SD
[mmim][MSO_4]	1.5338	-0.0002	0.9960	0.0007
[mmpyz][MSO_4]	1.5304	-0.0002	0.9949	0.0019
[mmpy][MSO_4]	1.6006	-0.0003	0.9767	0.0125
[mmpyrr][MSO_4]	1.5079	-0.0002	0.9854	0.0004
[bmim][DHP]	1.5444	-0.0005	0.9933	0.0057
[bmim][DMP]	1.5612	-0.0003	0.9892	0.0088
[bmim][DBP]	1.6577	-0.0003	0.9983	0.0020
[bmim][HSO_4]	1.5313	-0.0002	0.9961	0.0003
[bmim][MSO_4]	1.5493	-0.0002	0.9987	0.0042
[bmim][BSO_4]	1.5502	-0.0003	0.9921	0.0121
[bmim][OSO_4]	1.5809	-0.0004	0.9961	0.0101
[bmim][OTf]	1.5106	-0.0002	0.9969	0.0142
[bmim][NTf_2]	1.5255	-0.0003	0.9998	0.0086
[bmim][Ac]	1.5170	-0.0001	0.9658	0.0148
[bmim][TFA]	1.5014	-0.0003	0.9997	0.0343
[bmim][NO_3]	1.6355	-0.0004	0.9962	0.0105
[bmim][CNS]	1.5550	-0.0001	0.9917	0.0009
[bmim][Imd]	1.6609	-0.0005	0.9913	0.0059
[bmim][Pyd]	1.6688	-0.0008	0.9799	0.0158
[bmim][DCA]	1.6386	-0.0007	0.9984	0.0034
[bmim][BZT]	1.6567	-0.0004	0.9965	0.0159
[bmim][SCL]	1.6623	-0.0004	0.9987	0.0067
[bmim][TCM]	1.7129	-0.0004	0.9877	0.0121

4.4.3 Thermodynamic Properties Evaluation

The purpose of this evaluation is to contribute to such analyses by determining the thermodynamic properties (molecular volume, V_m, lattice potential energy, U_{POT} and absolute entropy, S_{298}) of ILs (*Glasser, 2004*), in order to provide information on their relative stabilities and to give a better understanding of these ILs that act as an extracting agent for diesel desulfurization. Their formulations have been given in previous chapter (Eq. 3.6, 3.7 and 3.8) and their resulting data are as follows, tabulated in Table 4.9.

Table 4.9: Calculated thermodynamic properties of 23 ILs

Ionic Liquid (ILs)	Density, ρ (g/cm^3)	Mol. weight, M_W (g/mol)	Mol. volume, V_m (nm^3)	Latt. pot. ener., U_{POT} (kJ/mol)	Abs. entropy, S_{298} (kJ/mol.K)
[mmim][MSO_4]	1.2980	208.24	0.2663	468.41	0.3615
[mmpyz][MSO_4]	1.3927	208.24	0.2482	477.07	0.3389
[mmpy][MSO_4]	1.4114	236.33	0.2780	463.25	0.3760
[mmPyrr][MSO_4]	1.3796	211.28	0.2542	474.11	0.3464
[bmim][DHP]	1.0822	236.21	0.3623	432.85	0.4811
[bmim][DMP]	1.0751	264.26	0.4080	420.08	0.5381
[bmim][DBP]	1.0372	348.42	0.5576	388.80	0.7246
[bmim][HSO_4]	1.2958	236.29	0.3027	453.18	0.4068
[bmim][MSO_4]	1.2082	250.32	0.3439	438.62	0.4582
[bmim][BSO_4]	1.1140	292.40	0.4357	413.23	0.5726
[bmim][OSO_4]	1.0606	348.51	0.5455	390.90	0.7094
[bmim][OTf]	1.2815	288.29	0.3734	429.56	0.4945
[bmim][NTf_2]	1.4343	422.38	0.4888	401.59	0.6388
[bmim][Ac]	1.0527	195.24	0.3079	451.21	0.4133
[bmim][TFA]	1.1980	252.23	0.3495	436.83	0.4652
[bmim][NO_3]	1.1539	201.22	0.2895	458.42	390.33
[bmim][CNS]	1.0704	197.31	0.3060	451.92	0.4109
[bmim][Imd]	1.1580	206.29	0.2957	455.90	0.3981
[bmim][Pyd]	1.1571	206.29	0.2959	455.81	0.3984
[bmim][DCA]	1.0581	205.26	0.3220	446.04	0.4309
[bmim][BZT]	1.0905	260.33	0.3963	423.17	0.5235
[bmim][SCL]	1.1515	276.33	0.3984	422.62	0.5261
[bmim][TCM]	1.0467	229.28	0.3636	432.46	0.4828

The molecular volume (V_m) of the ILs can be solely estimated from the experimental density data. As shown in Figure 4.9, the molecular volumes of phosphate-based ILs ([bmim][DHP], [bmim][DMP], [bmim][DBP]) and sulfate-based ILs ([bmim][HSO_4], [bmim][MSO_4], [bmim][BSO_4], [bmim][OSO_4]) behave in a regular manner whereby it increases with the increment of carbon number. The increment of 0.0491 or 0.02455 nm^3 per methylene (-CH_2-) group was observed for phosphate-based while for sulfate-based ILs, the increment was 0.0299 nm^3. These increment values agree well with the findings by Glasser, (2004) which demonstrated 0.0275 nm^3 per methylene group of both tetrafluoroborate-based and bis(trifluoromethanesulfonyl)imide-based ILs.

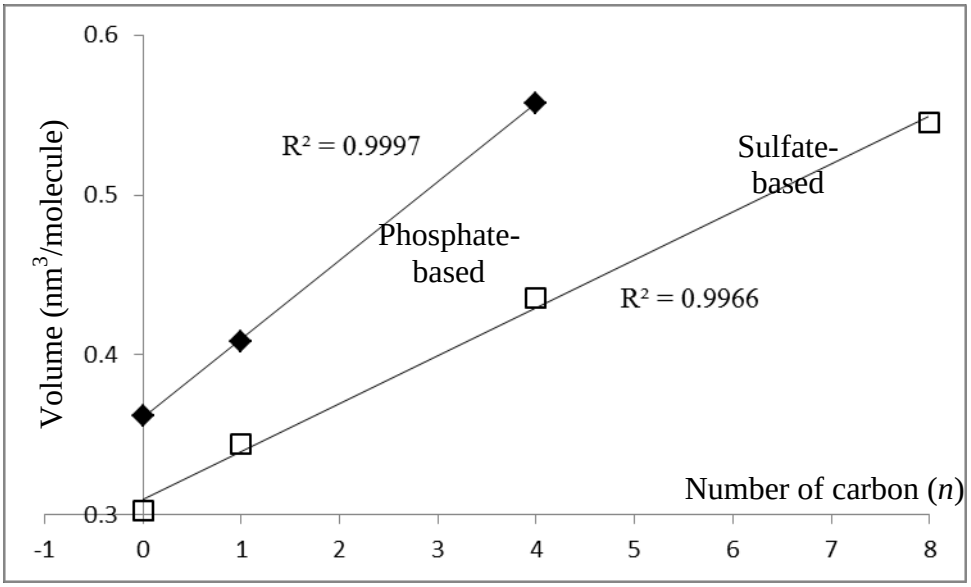

Figure 4.9: Molecular volume (nm^3/molecule) vs. number of carbon (*n*) for phosphate-based and sulfate-based ILs. The least square fitted equation are V_m (nm^3) = 0.0491*n* + 0.3609 for phosphate-based ILs and V_m (nm^3) = 0.0299*n* + 0.3096 for sulfate-based ILs

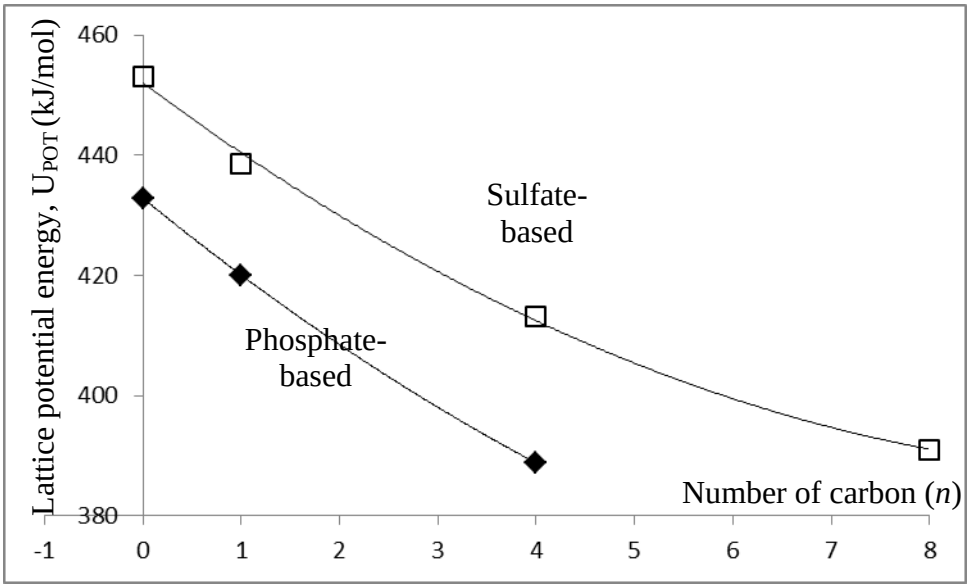

Figure 4.10: Lattice potential energy, U_{POT} vs. number of carbon (*n*) for phosphate-based and sulfate-based ILs

Figure 4.10 shows that there is a smooth, monotonic decrease in lattice potential energy with increasing alkyl chain length for both phosphate-based and sulfate-based ILs. Both series were observed to fit quadratic relationship very well. Estimating the lattice potential energy, U_{POT} may be helpful in assessing the relative stabilities of both phosphate-based and sulfate-based ILs, since as indicated here both group of ILs tend to decrease stability with increasing alkyl chain length. These are in good agreement with ab initio calculation of interaction energy of ILs, which demonstrated a decrease in interaction energy with increasing alkyl chain length of various ILs (*Zhou et al. 2008*).

Estimated entropies at ambient temperature, S_{298} of phosphate-based and sulfate-based ILs are plotted in Figure 4.11. Both series fit the linear relationship well and the values are in good agreement with reported literature (*Glasser, 2004*). The entropy contribution per methylene group of phosphate-based and sulfate-based ILs are 30.58 J/ (K.mol) and 37.32 J/(K.mol), respectively.

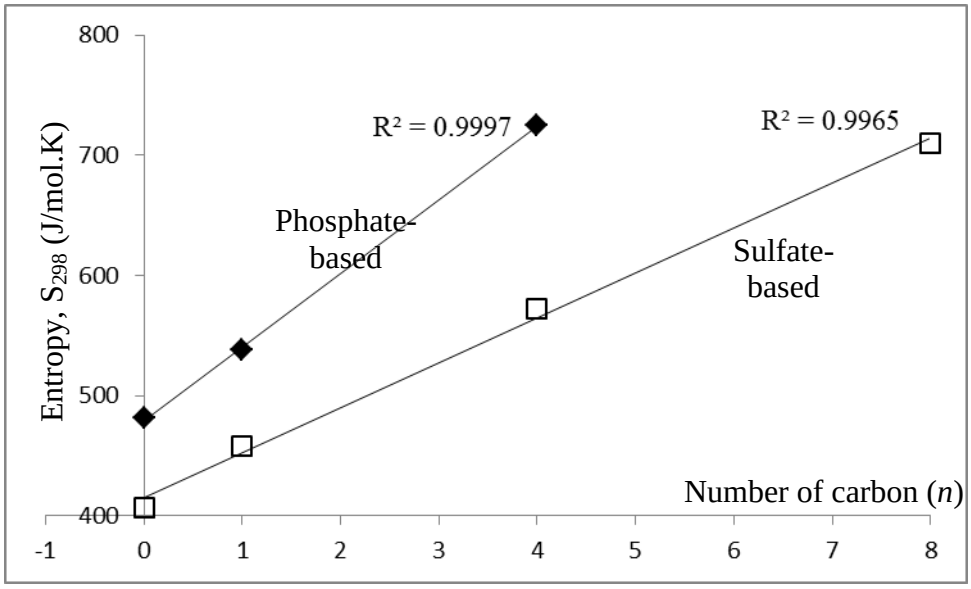

Figure 4.11: Entropy at ambient temperature, S_{298} vs. number of carbon (*n*) for phosphate-based and sulfate-based ILs

Although all 23 ILs were estimated for their thermodynamic properties, but only seven which belong to the two groups (phosphate-based and sulfate-based) are discussed. Others remained anomalous to be classified due to the scattered data.